Supplement of

The onset of the spring phytoplankton bloom in the coastal North Sea supports the Disturbance Recovery Hypothesis

Ricardo González-Gil[1*], Neil S. Banas[1], Eileen Bresnan[2], Michael R. Heath[1]

[1]Department of Mathematics and Statistics, University of Strathclyde, 26 Richmond Street, Glasgow, G1 1XH, UK
[2]Marine Scotland Science, Marine Laboratory, 375 Victoria Road, Aberdeen, AB11 9DB, UK

**Correspondence to*: Ricardo González-Gil (rgonzalezgil@gmail.com)

1 Supplementary Notes

1.1 Supplementary Note 1: Relationship between light attenuation (K_d) and Secchi disk depth (Z_{SD})

From 2007 to 2011, vertical light attenuation (K_d) profiles were weekly estimated at the Stonehaven site based on chlorophyll '*a*' (Chl) and turbidity profiles sampled using a Saiv SD204 CTD (Saiv A/S Environmental Sensors & Systems) equipped with a fluorescence and an optical backscatter sensor (for further methodological details, see Heath et al., 2017). As Secchi disk depths (Z_{SD}) were recorded weekly (Bresnan et al., 2016) during almost the entire period analyzed (2001 to 2017), we used Z_{SD} to calculate K_d. For this, we estimated the relationship between log-transformed Z_{SD} and K_d averaged from 0 to 10 m depth (the layer where phytoplankton was sampled) or averaged for the entire water column (i.e., 0 to 48 m; see Figure S1). In both cases, the coefficients of the relationship were similar and relatively close to those estimated by Devlin et al. (2008) for UK coastal waters. However, the proportion of variance explained by the relationship was larger when K_d was averaged for the 0–10 m layer. This makes sense considering that Z_{SD} records depend largely on the section of the attenuation profile above them and that the calculated average Z_{SD} between 2007 and 2011 was 6.61 ± 1.89 m (Mean ± SD); between 2001 and 2017, the average Z_{SD} was similar (6.94 ± 2.15 m).

1.2 Supplementary Note 2: Transformation of sunshine duration records into incoming solar radiation

Daily amounts of sunshine duration recorded at the Dyce meteorological station (57° 12.3' N, 2° 12.2' W, Met Office, 2012) were transformed into total incoming solar radiation ($W\ m^{-2}$) using the Ångström–Prescott model and site-dependent coefficients from Bojanowski et al. (2013). To estimate incoming solar radiations, we used the R packages suncalc v0.5.0 (Thieurmel and Elmarhraoui, 2019) and sirad v2.3-3 (Bojanowski, 2016).

After 2005 (a year without records), the Campbell–Stokes (C–S) recorder was replaced in 2006 by a new automatic Kipp and Zonen (KZ) sensor at Dyce, requiring a data correction to avoid any bias. Bojanowski et al. (2013) used sunshine data from

2005 to 2010, a period when all meteorological stations from eastern Scotland had KZ sensors (Legg, 2014). Thus, before estimating the incoming solar radiations, we converted C–S records prior to 2005 into KZ sunshine durations.

To convert C–S into KZ sunshine durations, we used information recorded between 2001 and 2005 at three meteorological stations of eastern Scotland (Kinloss, Aviemore, and Leuchars; see Legg, 2014 for more details). Following Legg (2014), we first converted sunshine durations measured by both sensors into proportions of maximum possible sunshine hours in a day. Then, we estimated the relationship between the proportions of maximum sunshine hours measured by each sensor for each day of the year (dy) using a generalized additive model (GAM, Hastie and Tibshirani, 1986):

$$KZ = a + te(CS, dy) + \varepsilon \quad \text{(S1)}$$

Where a represents the intercept, $te(CS, dy)$ is an interaction term included as a 2D smooth (in particular, a tensor product) that captures how the nonlinear effect of C–S sunshine proportions varies through the seasonal cycle (Wood, 2017), and ε is the error term. The tensor product had as marginal bases a thin-plate regression spline for CS and a cyclic cubic spline for dy, with maximum effective degrees of freedom (edf) set to 4 and 8, respectively, and optimal edf determined by restricted maximum likelihood, REML (Wood, 2017). We fitted the model using the R package mgcv v1.8-33 (Wood, 2017) and it had a p-value = 0.000 and $R^2 = 0.961$. Model predictions are shown in Figure S2 and also per month in Figure S3, for comparison with Legg (2014). Between April and August, this model predicted some negative proportions of KZ sunshine durations for the lowest C–S proportions (although never below -0.004). As negative proportions cannot occur, we set them to zero. Finally, KZ estimated proportions were converted back into hours of sunshine duration per day.

1.3 Supplementary Note 3: Estimation of surface and attenuated Photosynthetic Active Radiation (PAR)

To obtain daily amounts of PAR arriving to the water surface (PAR_{Sfc}), estimations of total incoming radiation (W m^{-2}) were multiplied by 0.43 (Baker and Frouin, 1987). To generate daily K_d for the 0–10 m layer ($K_{d,10}$) or for the entire water column ($K_{d,48}$), we linearly interpolated Z_{SD} between sampling dates before applying the linear models shown in Figure S1. Using daily estimations of PAR_{Sfc} and K_d, we calculated average attenuated PAR (PAR_{Att}) as:

$$PAR_{Att,z} = \frac{\int_0^z PAR_{Sfc}\, e^{-K_{d,z}\, z}\, dz}{z} \quad \text{(S2)}$$

where z is the depth of the layer for which PAR_{Att} was estimated (in our case 10 or 48 m). Finally, PAR_{Sfc} and PAR_{Att} estimated for both the 0–10 m layer ($PAR_{Att,10}$) and the entire water column ($PAR_{Att,48}$) were converted from W m^{-2} to µmol m^{-2} s^{-1} using a conversion factor of 0.217 W m^{-2} = 1 µmol m^{-2} s^{-1} (Carruthers et al., 2001).

1.4 Supplementary Note 4: Phytoplankton carbon (C) biomass calculations using microscopy and flow cytometry counts

To calculate phytoplankton C biomass concentrations (mg C m^{-3}) based on microscopic observations (2000–2017), we estimated the cell carbon content (C_c, pg C $cell^{-1}$) of the different phytoplankton taxa identified. For this, we collected cell volume information (V_c, μm^{-3}) from the literature (Table S1). Due to limitations in cell identification using a light microscope at x200 magnification, only diatom and dinoflagellate taxa with a mean cell diameter generally > 10 µm (Table S1) were extensively characterized and thus, we only gathered information for these groups.

Following Harrison et al. (2015), prior to statistical calculations, we transformed individual V_c to equivalent spherical diameter (ESD) using the below Eq. S3, as ESD shows a more normal distribution than V_c:

$$ESD = 2\left(\frac{3}{4}\frac{V_c}{\pi}\right)^{\frac{1}{3}} \quad \text{(S3)}$$

Then, after converting mean ESD to mean V_c using the reverse form of Eq. S3, we estimated mean C_c using the equation $C_c = aV_c{}^b$, where a and b are respectively 0.288 and 0.811 for diatoms, and 0.216 and 0.939 for non-diatom (Menden-Deuer and Lessard, 2000).

Finally, we estimated the C biomass for diatom and dinoflagellate taxa with a mean cell diameter usually > 10 µm ($C_{diatom+dinoflagellate\ >10\mu m}$). For this, we summed the observed cell abundance (n) multiplied by the corresponding C_c for all taxonomic entities (N):

$$C_{diatom+dinoflagellate\ >10\mu m} = \sum_{i=1}^{N} n_i \cdot C_c \quad \text{(S4)}$$

As the detection limit for microscopic phytoplankton counts was around 1 x 10^6 cells m^{-3}, there were several zero-abundance records and, consequently, several $C_{diatom+dinoflagellate\ >10\mu m} = 0$ mg C m^{-3}. To correct this, in those dates when zero-abundance records of diatoms or dinoflagellates were registered, we replaced zero-biomass concentrations for each class by half of their minimum biomass estimated throughout the entire time-series (i.e., half of the minimum $C_{diatom\ >10\mu m} > 0$ mg C m^{-3} or $C_{dinoflagellate\ >10\mu m} > 0$ mg C m^{-3}).

To calculate C biomass concentrations (mg C m^{-3}) using flow cytometer counts (2015–2017), we followed a similar procedure as the one used for microscope observations. In this case, to estimate for a particular date the C biomass of the different phytoplankton groups identified (which ESD rarely exceeded 10 µm), we multiplied their abundance by their representative cell carbon content (C_c, pg C $cell^{-1}$) extracted from the literature (Table S2).

1.5 Supplementary Note 5: Estimation of C biomass for the entire phytoplankton community (C_{phyto}) based on a C:Chl seasonality

Although Chl is extensively used as a proxy of phytoplankton biomass, changes in the concentration of this pigment are also driven by physiological adaptations to the environment (e.g., nutrient concentration and light availability). Thus, it is recommended to use carbon (C) phytoplankton biomass instead (Behrenfeld and Boss, 2018).

We could estimate C biomass of the entire phytoplankton community (C_{phyto}, mg C m^{-3}) using only cell counts from microscopic analysis and cell C contents based on size information from the literature (Supplementary Note 4 and Table S1). However, these estimations present some limitations compared to the use of Chl concentration as a proxy for phytoplankton biomass: 1) species counts at x200 magnification are only available since 2000 (Bresnan et al., 2016); 2) while Chl concentrations depend on phytoplankton encompassing all groups and sizes, only diatom and dinoflagellate taxa with average cell sizes generally > 10 µm (Table S1) were extensively characterized at the microscope due to limitations in cell identification at x200 magnification; 3) The detection limit for microscopic phytoplankton counts was around 1 x 10^6 cells m^{-3}, leading to several zero-abundance records for all taxa, especially in winter (although see supplementary Note 4); 4) using average cell sizes from the literature rather than in situ size measures might lead to less accurate C biomass estimations for a particular sampling date.

Alternatively, the use of flow cytometry counts and cell C contents from the literature to estimate C_{phyto} (Supplementary Note 4 and Table S2) would also present several issues. For instance, these data are only available since 2015 and phytoplankton cells counted with the flow cytometry rarely exceeded 10 µm.

Considering all the above, we decided to transform Chl concentrations into C_{phyto} using an average seasonality of C:Chl ratios estimated by combining the available information. However, for this estimation, we excluded 2017 as this year has several long data gaps and showed an unusually large *Phaeocystis* spp. bloom in October–December compared to the other years (Figure S4 and Figure 3 in the main text).

To estimate the average seasonal cycle of the C:Chl ratio at the Stonehaven monitoring site, we followed several steps. First, we estimated total C biomass of large (> 10 µm) diatoms and dinoflagellates ($C_{diatom+dinoflagellate >10µm}$) based on microscopic analysis and, since 2015, C biomass for the whole phytoplankton community (C_{phyto}) by adding $C_{diatom+dinoflagellate >10µm}$ to the C biomass of all the groups identified with the flow cytometer (Supplementary Note 4). Although some overlap might exist between the cell size ranges of the phytoplankton identified using the microscope and flow cytometer, we expect this to be small. Then, for 2015–2016, a model comparison showed that the same seasonal curve should be applied to the $C_{diatom+dinoflagellate >10µm}$:Chl and C_{phyto}:Chl ratios, with a difference of 23.747 in their intercepts (model 2 in Table S3 and Figure S4a). Finally, assuming that the difference in the intercept remains more or less constant among years and using data from 2000 to 2016, we fitted a seasonal curve to the $C_{diatom+dinoflagellate}$:Chl ratios and added 23.747 to obtain the average seasonality of C_{phyto}:Chl (Figure S4b). The shape of the seasonal curve is similar to the one described in Jakobsen and Markager (2016) for another coastal area of the North Sea, although our estimations are higher probably because we also accounted for the biomass of the small size (< 10 µm) phytoplankton.

2 Supplementary Figures

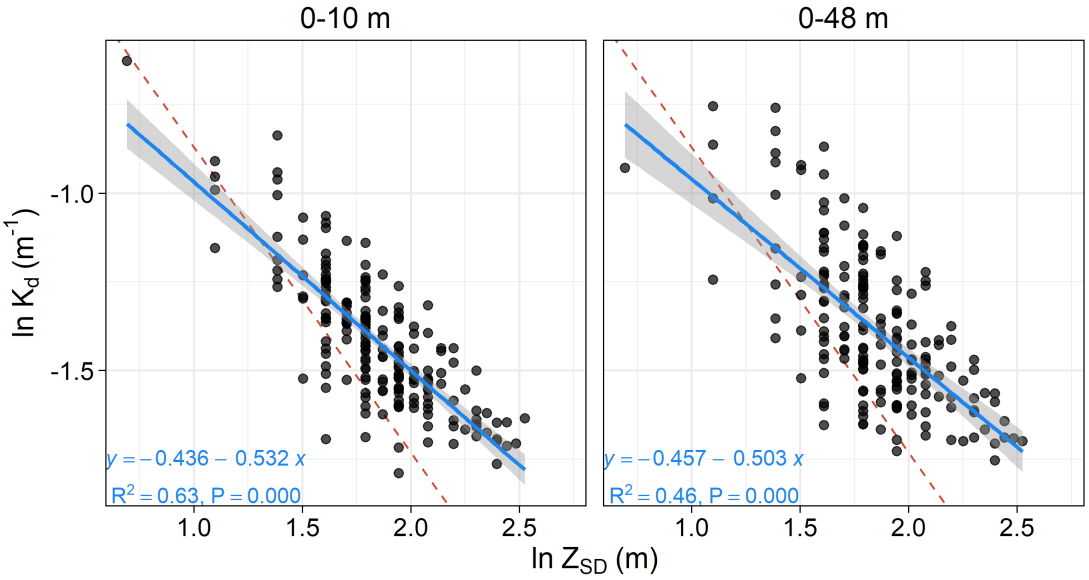

Figure S1. Relationship between log-transformed light attenuation coefficient (K_d) and Secchi disk depth (Z_{SD}). To estimate K_d, attenuation profiles (2007–2011) were averaged between the surface and 10 m depth (left panel) or for the entire water column (right panel). The shaded area represents the 95% confidence interval associated with the estimated linear correlation (blue line). The equation, proportion of variance explained (R^2), and p-value (P) of the relationships are shown. Additionally, the linear relationship estimated by Devlin et al. (2008) for UK coastal waters is also included (red dashed line).

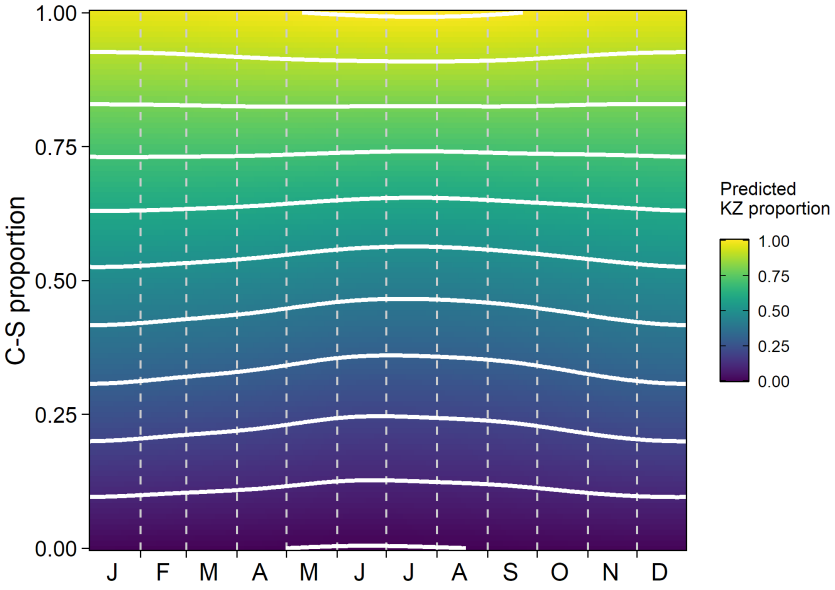

Figure S2. Predicted proportion of maximum possible sunshine-hours in a day measured by the automatic Kipp and Zonen (KZ) between 2001 and 2005 at three meteorological stations of eastern Scotland (Kinloss, Aviemore, Leuchars, see Legg, 2014 for more details). Predicted values were obtained using a generalized additive model (GAM) that included an interaction between the maximum possible sunshine-hours in a day measured by the Campbell–Stokes (C–S) and day of year (see Eq. S1).

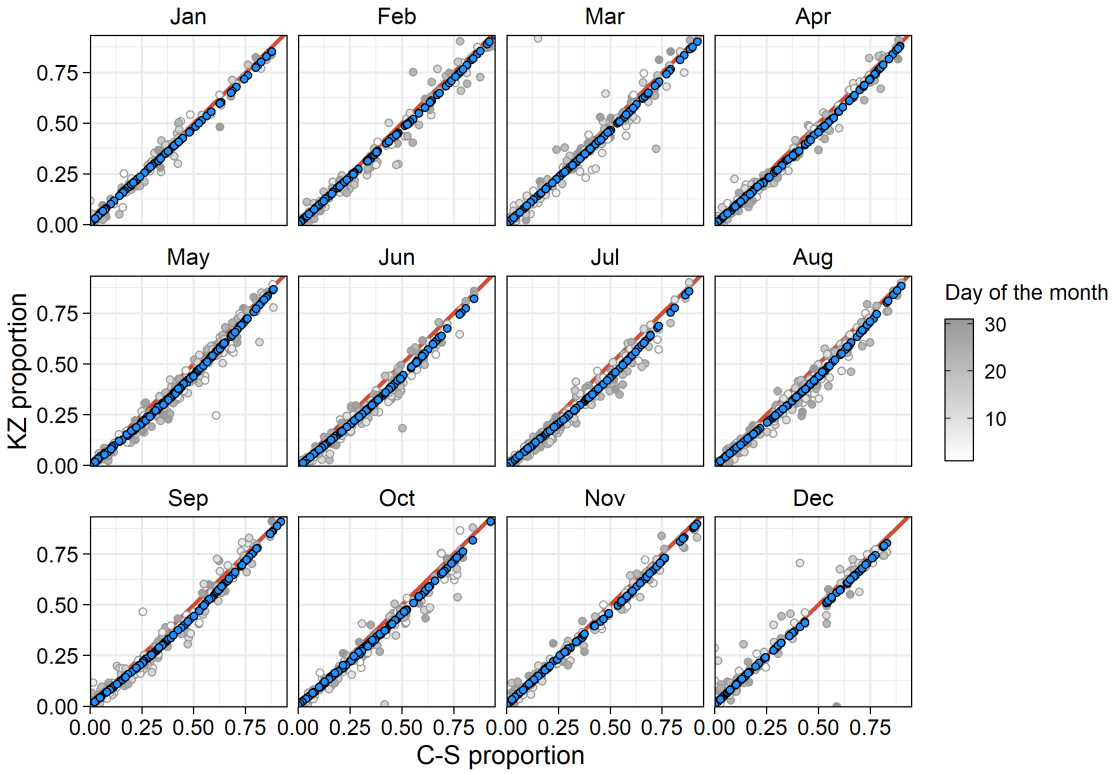

Figure S3. Relationship between maximum possible sunshine-hours in a day measured by the automatic Kipp and Zonen (KZ) and Campbell–Stokes (C–S) sensors for each month (grey filled dots). Records were made between 2001 and 2005 at three meteorological stations of eastern Scotland (Kinloss, Aviemore, Leuchars, see Legg, 2014 for more details). Blue dots correspond to the predicted maximum possible sunshine-hours in a day measured by the automatic Kipp and Zonen (KZ) shown in Figure S2 (see Eq. S1). We also show in red the 1:1 line for reference.

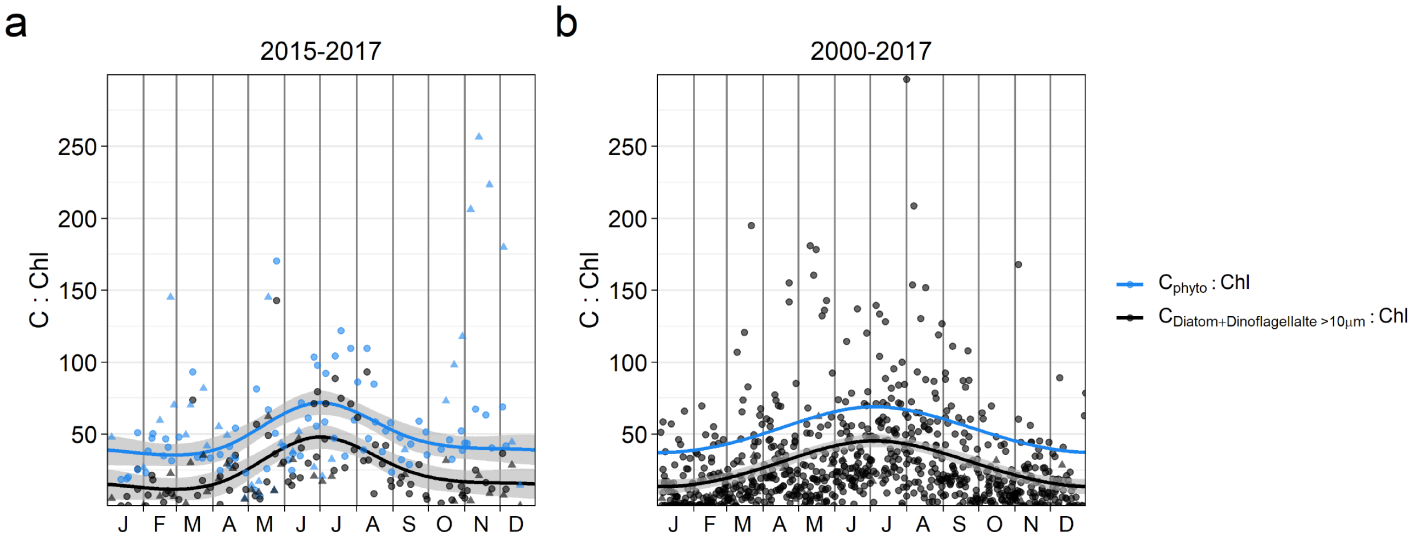

Figure S4. (a) C:Chl ratios (2015–2017) calculated using C biomass for the whole phytoplankton community (C_{phyto}, blue symbols) or C biomass of large (> 10 µm) diatoms and dinoflagellates ($C_{diatom+dinoflagellate >10\mu m}$, black symbols). Lines represent the estimated seasonality (2015–2016) based on the best generalized additive model (GAM) from Table S3, although fitted using restricted maximum likelihood, REML. (b) C:Chl ratios (2000–2017) calculated using C biomass of large (> 10 µm) diatoms and dinoflagellates ($C_{diatom+dinoflagellate >10\mu m}$, black symbols). The black line represents the estimated seasonality (2000–2016) based on the first GAM in Table S3, although fitted using REML. The blue line results from adding 23.747 to this seasonality, which is the difference in the intercept between the two curves shown in (a). In (a) and (b), triangles correspond to 2017 and dots to the rest of the years, and shaded areas denote the 95% confidence interval associated to the estimated seasonalities.

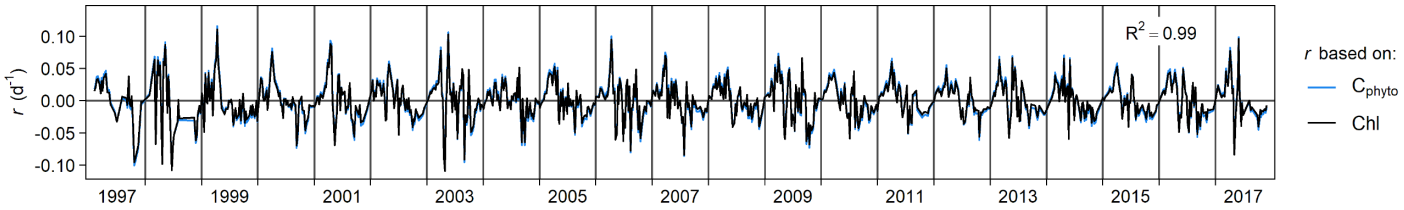

Figure S5. Changes through time in phytoplankton biomass accumulation rates (*r*, see Methods in the main text) based on estimated C biomass concentrations for the whole phytoplankton community (C_{phyto}, blue line) and based on Chl concentrations (black line). The proportion of variance explained (R^2) by the linear relationship between the two time series is also shown.

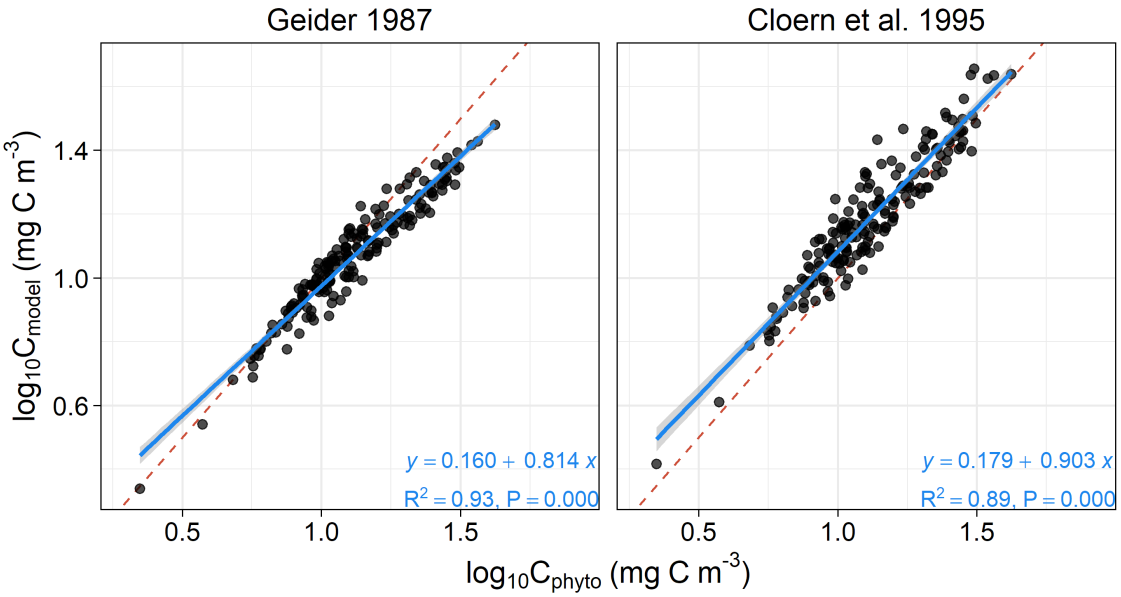

Figure S6. Relationship between log-transformed phytoplankton C biomass concentrations in winter (60 days before and after the winter solstice) estimated using two published C:Chl models, C_{model} (left panel, Geider, 1987; right panel, Cloern et al., 1995), and using the fixed C:Chl seasonality from this study, C_{phyto} (see Supplementary Note 5). To calculate C:Chl ratios, models are fed with estimated average attenuated Photosynthetic Active Radiations (PAR) for the whole water column (i.e., 0–48 m depth) and with temperature averaged between surface and bottom layers. The shaded area represents the 95% confidence interval associated with the estimated linear correlation (blue line). The equation, proportion of variance explained (R^2), and p-value (P) of the relationships are shown. We also show the 1:1 relationship (red dashed lines) for comparison.

125

3 Supplementary Tables

Table S1. Cell volume (V_c; µm^3) and equivalent spherical diameter (ESD; µm) information for the 85 species, 44 genera and 2 classes identified using a light microscope at 200X magnification. V_c was transformed into cell carbon content (C_c; pg C cell^{-1}) following Menden-Deuer and Lessard (2000) recommendations. The number of species aggregated for statistical calculations at genus or class level is indicated ($N_{species}$); NA denotes that the exact $N_{species}$ was not available. For some species, only information at genus level was available and, in those cases, the $N_{species}$ is shown. (a) Information from Harrison et al. (2015), hrr15; from Olenina et al. (2006), ol06; and from Leblanc et al. (2012), leb12. For all of these sources, minimum-maximum V_c were available. However, in the case of Leblanc et al. (2012), mean V_c corresponds to the mean of minimum-maximum V_c and therefore, no coefficient of variation (CV) is reported. Additionally, when Olenina et al. (2006) was the source, the number of individual cells used for calculations is shown (n). In general, we chose Harrison et al. (2015) over the other potential sources as the information given in this publication is based on several data sets from coastal areas. (b) For these species, only length information of cell axes (µm) was available. Using this information and selected cell shape formulas from Olenina et al. (2006), we calculated V_c. Only for Názan et al. (2012) and Gómez et al. (2016) minimum-maximum V_c were calculated and, in these cases, mean V_c is also reported.

Table S1a

Taxonomic level	name	$N_{species}$	n	Mean ESD	V_c min-max	Mean V_c (CV%)	Mean C_c	Comments	Source
Species									
	Bacillariophyceae								
	Achnanthes longipes	NA	15	10.72	150-2750	645 (26.9)	54.7		ol06
	Asterionellopsis glacialis			11.50	94-11300	797 (49.0)	64.9		hrr15
	Cerataulina pelagica			31.33	2840-102000	16100 (39.0)	743.2		hrr15
	Chaetoceros danicus			13.75	113-5080	1360 (33.0)	100.2		hrr15
	Chaetoceros socialis			8.79	33-3150	356 (45.0)	33.8		hrr15
	Corethron hystrix			57.78	2470-1420000	101000 (78.0)	3295.3		hrr15
	Cylindrotheca closterium			9.33	10-5230	425 (54.0)	39.0		hrr15
	Dactyliosolen fragilissimus			25.12	1680-143000	8300 (48.0)	434.3		hrr15
	Detonula confervacea			12.08	498-2140	922 (19.0)	73.1		hrr15
	Detonula pumila			28.48	2360-43700	12100 (28.0)	589.6		hrr15
	Ditylum brightwellii			51.95	28100-274000	73400 (22.0)	2543.7		hrr15
	Eucampia zodiacus			25.95	737-31800	9150 (28.0)	470.0		hrr15

Taxonomic level	name	$N_{species}$	n	Mean ESD	V_c min-max	Mean V_c (CV%)	Mean C_c	Comments	Source
	Guinardia delicatula			22.51	831-26600	5970 (30.0)	332.4		hrr15
	Guinardia flaccida			63.49	16600-349000	134000 (26.0)	4144.5		hrr15
	Guinardia striata			40.85	2770-201000	35700 (35.0)	1417.8		hrr15
	Leptocylindrus danicus			16.45	95-10400	2330 (30.0)	155.0		hrr15
	Leptocylindrus mediterraneus			26.91	382-68200	10200 (51.0)	513.3		hrr15
	Leptocylindrus minimus			8.41	10-3380	312 (53.0)	30.3		hrr15
	Meuniera membranacea			50.12	18850-159043	65923	2331.5		leb12
	Nitzschia longissima			10.46	24-15400	599 (63.0)	51.5		hrr15
	Paralia sulcata			23.65	1150-68000	6930 (43.0)	375.2		hrr15
	Proboscia alata			34.50	281-306000	21500 (55.0)	939.7		hrr15
	Proboscia indica	1		34.50	281-306000	21500 (55.0)	939.7		hrr15
	Rhizosolenia hebetata			47.78	439-188000	57100 (46.0)	2075.0		hrr15
	Rhizosolenia imbricata			54.12	1360-1560000	83000 (67.0)	2810.4		hrr15
	Rhizosolenia setigera			32.52	1480-150000	18000 (44.0)	813.6		hrr15
	Rhizosolenia styliformis			69.53	18900-1290000	176000 (48.0)	5170.2		hrr15
	Stephanopyxis turris			32.58	6840-47700	18100 (22.0)	817.3		hrr15
	Striatella unipunctata			52.40	5773-294524	75345	2598.3		leb12
	Thalassionema nitzschioides			13.33	50-143000	1240 (80.0)	92.9		hrr15
	Thalassiosira nordenskioeldii			30.87	193-499000	15400 (79.0)	716.9		hrr15
	Thalassiosira rotula			28.40	3450-47000	12000 (25.0)	585.6		hrr15
	Dinophycea								

Taxonomic level	name	$N_{species}$	n	Mean ESD	V_c min-max	Mean V_c (CV%)	Mean C_c	Comments	Source
	Amphidinium crassum	NA	16	16.69	92-19852	2434 (46.1)	326.7		ol06
	Amphidinium sphenoides	NA	16	16.69	92-19852	2434 (46.1)	326.7		ol06
	Amylax triacantha			27.51	4600-16800	10900 (13.0)	1335.4		hrr15
	Archaeperidinium minutum			30.25	25-41600	14500 (40.0)	1745.7		hrr15
	Dinophysis acuminata			27.25	1670-40700	10600 (26.0)	1300.8		hrr15
	Dinophysis acuta			43.73	1580-105000	43800 (29.0)	4929.4		hrr15
	Dinophysis dens	5		43.13	10700-54400	42000 (7.7)	4739.0		hrr15
	Gonyaulax digitalis			32.27	2950-43400	17600 (21.0)	2094.1		hrr15
	Gonyaulax spinifera			31.33	10700-23800	16100 (9.0)	1926.0		hrr15
	Gonyaulax verior			28.33	7120-39300	11900 (23.0)	1450.1		hrr15
	Gyrodinium fusiforme			32.58	3520-109000	18100 (35.0)	2149.9		hrr15
	Gyrodinium lachryma	NA	30	35.10	72-177606	22637 (43.3)	2652.4		ol06
	Gyrodinium spirale			36.61	3160-113000	25700 (38.0)	2988.0		hrr15
	Heterocapsa niei	NA	18	11.45	103-4179	785 (40.7)	113.0		ol06
	Heterocapsa triquetra			16.75	965-5700	2460 (16.0)	330.0		hrr15
	Karenia mikimotoi	NA	35	29.14	72-177606	12958 (64.2)	1570.8	It belongs to the order Gymnodiniales. Thus, we used information for *Gymnodinium* spp., which have a similar cell shape.	ol06
	Katodinium glaucum			17.19	416-18300	2660 (38.0)	355.2		hrr15
	Oxyrrhis marina			15.81	268-6370	2070 (34.0)	280.6		hrr15
	Oxytoxum gracilis	1		7.81	78-476	249 (20.0)	38.4		hrr15

Taxonomic level	name	$N_{species}$	n	Mean ESD	V_c min-max	Mean V_c (CV%)	Mean C_c	Comments	Source
	Pentapharsodinium dalei		3	14.02	497-3454	1443 (32.0)	200.0		ol06
	Phalacroma oxytoxoides	1		32.15	499-116000	17400 (41.0)	2071.7		hrr15
	Phalacroma rotundatum			32.15	499-116000	17400 (41.0)	2071.7		hrr15
	Polykrikos schwartzii			64.27	27300-293000	139000 (28.0)	14579.6		hrr15
	Prorocentrum compressum	5		13.37	905-9740	1250 (6.3)	174.8		hrr15
	Prorocentrum micans			23.92	71-18600	7170 (31.0)	901.1		hrr15
	Prorocentrum minimum	5		13.37	905-9740	1250 (6.3)	174.8		hrr15
	Protoceratium reticulatum			31.20	7450-31300	15900 (15.0)	1903.6		hrr15
	Protoperidinium bipes			16.06	432-3650	2170 (18.0)	293.4		hrr15
	Protoperidinium brevipes			26.82	5450-14900	10100 (12.0)	1243.1		hrr15
	Protoperidinium cerasus	17		51.38	11400-455000	71000 (17.0)	7758.6		hrr15
	Protoperidinium conicoides			43.83	10700-103000	44100 (25.0)	4961.1		hrr15
	Protoperidinium conicum			57.47	6060-345000	99400 (28.0)	10641.4		hrr15
	Protoperidinium crassipes			73.39	81300-606000	207000 (29.0)	21190.9		hrr15
	Protoperidinium curtipes	17		51.38	11400-455000	71000 (17.0)	7758.6		hrr15
	Protoperidinium depressum			89.63	21900-1330000	377000 (29.0)	37208.2		hrr15
	Protoperidinium excentricum	17		51.38	11400-455000	71000 (17.0)	7758.6		hrr15
	Protoperidinium mite	17		51.38	11400-455000	71000 (17.0)	7758.6		hrr15
	Protoperidinium ovatum	17		51.38	11400-455000	71000 (17.0)	7758.6		hrr15
	Protoperidinium pallidum			51.38	2620-244000	71000 (33.0)	7758.6		hrr15
	Protoperidinium pellucidum			38.42	6800-78800	29700 (22.0)	3422.7		hrr15
	Protoperidinium steinii			33.45	9160-58900	19600 (21.0)	2316.8		hrr15

Taxonomic level	name	$N_{species}$	n	Mean ESD	V_c min-max	Mean V_c (CV%)	Mean C_c	Comments	Source
	Protoperidinium subinerme	17		51.38	11400-455000	71000 (17.0)	7758.6		hrr15
	Pyrophacus horologium			43.70	8890-182000	43700 (39.0)	4918.9		hrr15
	Scrippsiella trochoidea			20.83	690-16800	4730 (28.0)	609.7		hrr15
	Torodinium robustum			18.86	1770-10600	3510 (19.0)	460.8		hrr15
	Tripos furca			44.84	3000-123000	47200 (26.0)	5287.9		hrr15
	Tripos fusus			38.34	6260-283000	29500 (40.0)	3401.1		hrr15
	Tripos horridus	9		42.82	13700-70700	41100 (7.6)	4643.6		hrr15
	Tripos lineatus			29.76	1110-96300	13800 (32.0)	1666.5		hrr15
	Tripos minutum	9		42.82	13700-70700	41100 (7.6)	4643.6		hrr15
	Tripos muelleri			49.42	414-814000	63200 (54.0)	6955.5		hrr15
Genus									
	Bacillariophyceae								
	Asterionella	3		14.28	235-4783	1525	109.9		leb12
	Bacteriastrum	1		28.64	1560-41000	12300 (38.0)	597.5	Information for *B. hyalinum*, present in the North Sea (Hoppenrath, 2004)	hrr15
	Bellerochea	1		42.04	1360-523000	38900 (77.0)	1520.0		hrr15
	Biddulphia	1		58.53	7790-440000	105000 (49.0)	3400.8		hrr15
	Cerataulina	1		31.33	2840-102000	16100 (39.0)	743.2		hrr15
	Chaetoceros	35		17.40	25-13200	2760 (6.7)	177.8		hrr15
	Coscinodiscus	7		123.66	4380-5580000	990000 (75.0)	20982.3		hrr15
	Detonula	NA		40.38	424-190852	34468	1378.0		leb12

Taxonomic level	name	$N_{species}$	n	Mean ESD	V_c min-max	Mean V_c (CV%)	Mean C_c	Comments	Source
	Eucampia	1		25.95	737-31800	9150 (28.0)	470.0		hrr15
	Fragilaria	NA	13	10.24	69-1581	563 (27.0)	49.0		ol06
	Guinardia	3		40.85	4580-163000	35700 (24.0)	1417.8		hrr15
	Gyrosigma/Pleurosigma	6	15	40.77	2457-211680	35472 (45.2)	1410.4		ol06
	Lauderia	1		37.27	13500-137000	27100 (24.0)	1133.8		hrr15
	Licmophora	NA		14.77	101-7020	1688	119.3		leb12
	Melosira	3		26.99	4580-22800	10300 (7.9)	517.4		hrr15
	Nitzschia	NA	20	13.48	45-29160	1282 (58.7)	95.5		ol06
	Odontella	1		33.79	919-148000	20200 (48.0)	893.4		hrr15
	Pseudo-nitzschia	3		12.92	200-1290	1130 (3.5)	86.2		hrr15
	Rhaphoneis	1		28.72	3240-31250	12403	601.5		leb12
	Rhizosolenia	4		50.96	10800-111000	69300 (14.0)	2427.9		hrr15
	Skeletonema	1		8.97	50-1810	378 (35.0)	35.5		hrr15
	Thalassionema	1		13.33	50-143000	1240 (80.0)	92.9	Information for *T. nitzschioides*	hrr15
	Thalassiosira	10		29.97	54-87100	14100 (15.0)	667.4		hrr15
	Triceratium	NA		82.12	64-2116273	289990	7751.5		leb12
	Dinophycea								
	Alexandrium	3		28.95	5810-38800	12700 (10.0)	1541.4		hrr15
	Amphidinium	NA	16	16.69	92-19852	2434 (46.1)	326.7		ol06
	Dinophysis	5		43.13	10700-54400	42000 (7.7)	4739.0		hrr15

Taxonomic level	name	$N_{species}$	n	Mean ESD	V_c min-max	Mean V_c (CV%)	Mean C_c	Comments	Source
	Diplopsalis	1		40.35	10800-106000	34400 (24.0)	3929.0		hrr15
	Gonyaulax	5		32.27	8080-25900	17600 (4.2)	2094.1		hrr15
	Gymnodinium	NA	35	29.14	72-177606	12958 (64.2)	1570.8		ol06
	Gyrodinium	NA	30	35.10	72-177606	22637 (43.3)	2652.4		ol06
	Heterocapsa	NA	18	11.45	103-4179	785 (40.7)	113.0		ol06
	Katodinium	1		17.19	416-18300	2660 (38.0)	355.2		hrr15
	Mesoporos	1		15.91	1150-3940	2110 (17.0)	285.7		hrr15
	Oblea	1		24.88	4190-14100	8060 (14.0)	1005.8		hrr15
	Oxytoxum	1		7.81	78-476	249 (20.0)	38.4		hrr15
	Polykrikos	1		64.27	27300-293000	139000 (28.0)	14579.6		hrr15
	Pronoctiluca	1		19.29	905-10500	3760 (29.0)	491.5		hrr15
	Prorocentrum	5		13.37	905-9740	1250 (6.3)	174.8		hrr15
	Protoperidinium	17		51.38	11400-455000	71000 (17.0)	7758.6		hrr15
	Scrippsiella	1		20.83	690-16800	4730 (28.0)	609.7		hrr15
	Tripos	9		42.82	13700-70700	41100 (7.6)	4643.6		hrr15
Class									
	Bacillariophyceae	114		35.08	27-5480000	22600 (107.0)	978.5		hrr15
	Dinophycea	79		33.16	177-377000	19100 (50.0)	2261.2		hrr15

Table S1b

Taxonomic level	name	ESD or mean ESD	V_c min-max	V_c or mean V_c	C_c or mean C_c	Comments (d, d1, d2 and h are dimensions in µm)	Source
Species							
	Bacillariophyceae						
	Mediopyxis helysia	54.18		83252	2817.3	-Dimensions: 100 (d1), 20 (d2) and 53 (h) -Geometric shape: oval cylinder	Kühn et al. (2006)
	Dinophycea						
	Azadinium caudata	19.87	2422-6430	4106	533.9	-Dimension ranges for Sottish waters: 18.9-25.8 (d) and 25.9-36.9 (h) -Geometric shape: Cone with half sphere	Nézan et al. (2012)
Genus	**Bacillariophyceae**						
	Lennoxia	4.18		38	5.5	-Mean dimensions from Greenland and Danish waters: 1.5 (d) and 65 (h) -Geometric shape: Double cone	Thomsen et al. (1993)
	Dinophycea						
	Corythodinium	42.50	8181-113097	40194	4547.4	-Dimension ranges (approximated): 25-60 (d) and 50-120 (h) -Geometric shape: Cone with half sphere	Gómez et al. (2016)

Table S2. Cell carbon content (C_c; pg C cell^{-1}) information for the different phytoplankton groups identified using a flow cytometer.

Phytoplankton group	C_c	Comments and Source
***Synechococcus* spp.**	0.1	Zubkov et al. (1998)
Pico-eukaryotes (0.2–2 µm)	1.5	Zubkov et al. (1998)
Nano-eukaryotes (2–10 µm)	24.9	Assuming an equivalent spherical diameter (ESD) of 6 µm (Pan et al., 2007), we estimated a cell volume (V_c) of 113 µm^3. Then, we transformed V_c into C_c using a conversion factor of 0.22 pg C µm^{-3} (Booth, 1988).
Coccolithophores	16.3	As *Emiliania huxleyi* is the dominant coccolithophore species in shelf areas of the North Sea (Charalampopoulou et al., 2011; Poulton et al., 2014), we transformed its mean V_c of 100 µm^3 (Harrison et al., 2015) into C_c following the conversion factor recommended by Menden-Deuer and Lessard (2000).
Cryptophytes	23.7	We transformed the mean V_c of 149 µm^3 for the class Cryptophyceae (Harrison et al., 2015) into C_c following the conversion factor recommended by Menden-Deuer and Lessard (2000).
***Phaeocystis* spp. single cells**	13.5	Rousseau et al. (1990)

Table S3: Results for different models to describe the effect of day of year (*dy*) on C:Chl ratios based on information from years 2015 and 2016 (see Supplementary Note 5 and Figure S4a). The categorical variable *group* has two levels, one corresponds to C biomass estimations for the whole phytoplankton community (C_{phyto}) and the other only for large (> 10 µm) diatoms and dinoflagellates ($C_{diatom+dinoflagellate\ >10µm}$). All models include an intercept (a) and an error term (ε). Additionally, the generalized additive models (GAMs) can include the effect of predictors through 1D smooth function (f) or an interaction term *f(dy|group)* to allow a different seasonality for each group. The smooth function (f) corresponds to a cyclic cubic spline with maximum effective degrees of freedom (***edf***) set to 5, and optimal ***edf*** determined by maximum likelihood, ML (Wood, 2017). For each model, we show the Akaike Information Criterion (AIC) and its associated weight (Burnham and Anderson, 2002), and the proportion of variance explained (R^2). In all cases, the overall model had a p-value < 0.001. The results for the model with the lowest AIC (model 2) are in bold.

Model	Model description	AIC	AIC weight	R^2
(1) $C: Chla = a + f(dy) + \varepsilon$	Effect of day of year	1488.86	0.00	0.207
(2) $C: Chla = a + group + f(dy) + \varepsilon$	Effect of day of year and different intercept for each group level	**1453.76**	**0.92**	**0.374**
(3) $C: Chla = a + f(dy\|group) + \varepsilon$	Effect of different day of the year for each group level	1458.72	0.08	0.374

4 References

Baker, K. S. and Frouin, R.: Relation between photosynthetically available radiation and total insolation at the ocean surface under clear skies, Limnol. Oceanogr., 32, 1370-1377, doi: 10.4319/lo.1987.32.6.1370, 1987.

Behrenfeld, M. J. and Boss, E. S.: Student's tutorial on bloom hypotheses in the context of phytoplankton annual cycles, Glob. Change Biol., 24, 55-77, doi: 10.1111/gcb.13858, 2018.

Bojanowski, J. S.: sirad: Functions for Calculating Daily Solar Radiation and Evapotranspiration. R package version 2.3-3, available at: https://CRAN.R-project.org/package=sirad, 2016.

Bojanowski, J. S., Vrieling, A., and Skidmore, A. K.: Calibration of solar radiation models for Europe using Meteosat Second Generation and weather station data, Agric. For. Meteorol., 176, 1-9, doi: 10.1016/j.agrformet.2013.03.005, 2013.

Booth, B. C.: Size classes and major taxonomic groups of phytoplankton at two locations in the subarctic pacific ocean in May and August, 1984, Mar. Biol., 97, 275-286, doi: 10.1007/BF00391313, 1988.

Bresnan, E., Cook, K., Hindson, J., Hughes, S., Lacaze, J.-P., Walsham, P., Webster, L., and Turrell, W. R.: The Scottish Coastal Observatory 1997-2013. Part 2 - Description of Scotland's Coastal Waters, Scott. Mar. Freshw. Sci., 7, 1-278, doi: 10.7489/1881-1, 2016.

Burnham, K. P. and Anderson, D. R.: Model selection and multimodel inference: a practical information-theoretic approach, Springer-Verlag, New York, 2002.

Carruthers, T. J. B., Longstaff, B. J., Dennison, W. C., Abal, E. G., and Aioi, K.: Chapter 19 - Measurement of light penetration in relation to seagrass, in: Global Seagrass Research Methods, edited by: Short, F. T., and Coles, R. G., Elsevier Science, Amsterdam, 369-392, doi: 10.1016/B978-044450891-1/50020-7, 2001.

Charalampopoulou, A., Poulton, A. J., Tyrrell, T., and Lucas, M. I.: Irradiance and pH affect coccolithophore community composition on a transect between the North Sea and the Arctic Ocean, Mar. Ecol. Prog. Ser., 431, 25-43, doi: 10.3354/meps09140, 2011.

Cloern, J. E., Grenz, C., and Vidergar-Lucas, L.: An empirical model of the phytoplankton chlorophyll : carbon ratio-the conversion factor between productivity and growth rate, Limnol. Oceanogr., 40, 1313-1321, doi: 10.4319/lo.1995.40.7.1313, 1995.

Devlin, M. J., Barry, J., Mills, D. K., Gowen, R. J., Foden, J., Sivyer, D., and Tett, P.: Relationships between suspended particulate material, light attenuation and Secchi depth in UK marine waters, Estuar. Coast. Shelf Sci., 79, 429-439, doi: 10.1016/j.ecss.2008.04.024, 2008.

Geider, R. J.: Light and Temperature Dependence of the Carbon to Chlorophyll a Ratio in Microalgae and Cyanobacteria: Implications for Physiology and Growth of Phytoplankton, New Phytol., 106, 1-34, doi: 10.1111/j.1469-8137.1987.tb04788.x, 1987.

Gómez, F., Wakeman, K. C., Yamaguchi, A., and Nozaki, H.: Molecular Phylogeny of the Marine Planktonic Dinoflagellate *Oxytoxum* and *Corythodinium* (Peridiniales, Dinophyceae), Acta Protozool., 55, doi: 10.4467/16890027AP.16.026.6095, 2016.

Harrison, P. J., Zingone, A., Mickelson, M. J., Lehtinen, S., Ramaiah, N., Kraberg, A. C., Sun, J., McQuatters-Gollop, A., and Jakobsen, H. H.: Cell volumes of marine phytoplankton from globally distributed coastal data sets, Estuar. Coast. Shelf Sci., 162, 130-142, doi: 10.1016/j.ecss.2015.05.026, 2015.

Hastie, T. J. and Tibshirani, R. J.: Generalized additive models, Stat. Sci., 1, 297-310, doi: 10.1214/ss/1177013604, 1986.

Heath, M., Sabatino, A., Serpetti, N., McCaig, C., and O'Hara Murray, R.: Modelling the sensitivity of suspended sediment profiles to tidal current and wave conditions, Ocean Coast. Manage., 147, 49-66, doi: 10.1016/j.ocecoaman.2016.10.018, 2017.

Hoppenrath, M.: A revised checklist of planktonic diatoms and dinoflagellates from Helgoland (North Sea, German Bight), Helgol. Mar. Res., 58, 243-251, doi: 10.1007/s10152-004-0190-6, 2004.

Jakobsen, H. H. and Markager, S.: Carbon-to-chlorophyll ratio for phytoplankton in temperate coastal waters: Seasonal patterns and relationship to nutrients, Limnol. Oceanogr., 61, 1853-1868, doi: 10.1002/lno.10338, 2016.

Kühn, S. F., Klein, G., Halliger, H., Hargraves, P., and Medlin, L.: A new diatom, *Mediopyxis helysia* gen. nov. and sp. nov. (Mediophyceae) from the North Sea and the Gulf of Maine as determined from morphological and phylogenetic characteristics, Nova Hedwig. Beih., 130, 307-324, 2006.

Leblanc, K., Arístegui, J., Armand, L., Assmy, P., Beker, B., Bode, A., Breton, E., Cornet, V., Gibson, J., Gosselin, M. P., Kopczynska, E., Marshall, H., Peloquin, J., Piontkovski, S., Poulton, A. J., Quéguiner, B., Schiebel, R., Shipe, R., Stefels, J., van Leeuwe, M. A.,

Varela, M., Widdicombe, C., and Yallop, M.: A global diatom database – abundance, biovolume and biomass in the world ocean, Earth Syst. Sci. Data, 4, 149-165, doi: 10.5194/essd-4-149-2012, 2012.

Legg, T.: Comparison of daily sunshine duration recorded by Campbell–Stokes and Kipp and Zonen sensors, Weather, 69, 264-267, doi: 10.1002/wea.2288, 2014.

Menden-Deuer, S. and Lessard, E. J.: Carbon to volume relationships for dinoflagellates, diatoms, and other protist plankton, Limnol. Oceanogr., 45, 569-579, doi: 10.4319/lo.2000.45.3.0569, 2000.

Met Office: Met Office Integrated Data Archive System (MIDAS) Land and Marine Surface Stations Data (1853-current), NCAS British Atmospheric Data Centre, 2021 [dataset], 2012.

Nézan, E., Tillmann, U., Bilien, G. l., Boulben, S., Chèze, K., Zentz, F., Salas, R., and Chomérat, N.: Taxonomic revision of the dinoflagellate *Amphidoma caudata*: transfer to the genus *Azadinium* (Dinophyceae) and proposal of two varieties, based on morphological and molecular phylogenetic analyses, J. Phycol., 48, 925-939, doi: 10.1111/j.1529-8817.2012.01159.x, 2012.

Olenina, I., Hajdu, S., Edler, L., Andersson, A., Wasmund, N., Göbel, J., Huttunen, M., Jaanus, A., Ledaine, I., Huseby, S., and Niemkiewicz, E.: Biovolumes and size-classes of phytoplankton in the Baltic Sea. *HELCOM*, Balt. Sea Environ. Proc., 106, 1–144, 2006.

Pan, L. A., Zhang, J., and Zhang, L. H.: Picophytoplankton, nanophytoplankton, heterotrohpic bacteria and viruses in the Changjiang Estuary and adjacent coastal waters, J. Plankton Res., 29, 187-197, doi: 10.1093/plankt/fbm006, 2007.

Poulton, A. J., Stinchcombe, M. C., Achterberg, E. P., Bakker, D. C. E., Dumousseaud, C., Lawson, H. E., Lee, G. A., Richier, S., Suggett, D. J., and Young, J. R.: Coccolithophores on the north-west European shelf: calcification rates and environmental controls, Biogeosciences, 11, 3919-3940, doi: 10.5194/bg-11-3919-2014, 2014.

Rousseau, V., Mathot, S., and Lancelot, C.: Calculating carbon biomass of *Phaeocystis* sp. from microscopic observations, Mar. Biol., 107, 305-314, doi: 10.1007/BF01319830, 1990.

Thieurmel, B. and Elmarhraoui, A.: suncalc: Compute Sun Position, Sunlight Phases, Moon Position and Lunar Phase. R package version 0.5.0, available at: https://CRAN.R-project.org/package=suncalc, 2019.

Thomsen, H. A., Buck, K. R., Marino, D., Sarno, D., Hansen, L. E., Østergaard, J. B., and Krupp, J.: Lennoxia faveolata gen. et sp. nov. (Diatomophyceae) from South America, California, West Greenland and Denmark, Phycologia, 32, 278-283, doi: 10.2216/i0031-8884-32-4-278.1, 1993.

Wood, S. N.: Generalized additive models: an introduction with R (2nd edition), Chapman and Hall/CRC, 2017.

Zubkov, M. V., Sleigh, M. A., Tarran, G. A., Burkill, P. H., and Leakey, R. J. G.: Picoplanktonic community structure on an Atlantic transect from 50°N to 50°S, Deep Sea Res. Part I Oceanogr. Res. Pap., 45, 1339-1355, doi: 10.1016/S0967-0637(98)00015-6, 1998.